J Eng Math (2008) 61:301–313
DOI 10.1007/s10665-008-9231-5

Forced response of cylindrical shells coupled with nonlinear shape-memory-alloy (SMA) actuators regulated by sinusoidal and saw-tooth temperature profiles

J. G. DeHaven · H. S. Tzou

Received: 14 November 2006 / Accepted: 14 December 2007 / Published online: 29 April 2008

Abstract Dynamic responses of cylindrical shells coupled with shape-memory alloy (SMA) ring segments placed at critical locations are investigated. Since the SMA actuators are highly nonlinear and governed by the temperate-dependent stiffness and martensite/austenite fraction, input shaping and phase shift of temperature profiles are incorporated to control the shell vibrations. Open-loop equations of an elastic cylindrical shell panel are defined first and then used with assumed mode-shape functions satisfying specified boundary conditions in the free-vibration analysis. Modal-analysis data are used to determine spatial strain distributions of natural modes. Distributed modal-signal characteristics suggest optimal placements of SMA actuator segment(s) for each given mnth mode. Based on the modal-expansion method, the open-loop control force induced by the SMA ring segments applied to a simply supported cylindrical shell panel is formulated. This formulation indicates that only the odd modes in the circumferential direction can be controlled. Longitudinal modes are controlled via placing specific number, depending on the mode, of actuator segments along the panel length. To predict control effects of the nonlinear SMA ring segments, the modal participation factor response is determined for an external harmonic excitation applied to the shell along with induced SMA control forces, via sinusoidal and saw-tooth temperature profiles to generate desirable control forces and to eliminate the unwanted effects. Analysis results suggest that with proper choice of temperature waveform function to the SMA ring segments and minor modifications to frequency and phase, the SMA ring segments can attenuate unwanted external vibrations of cylindrical shells.

Keywords Input shaping · Open-loop · Ring actuators · Shape-memory alloy · Vibration control

1 Introduction

There have been a variety of engineering systems employing smart materials to create active and adaptive systems, e.g., smart structures and structronic systems, which can sense changes in the environment and make modifications when and where they are needed. Shape-memory alloys (SMAs) have become a popular material to use in such systems because of the large forces generated during the phase transformation and its excellent recovery of large strains. Recent developments of shape control include shape-changing airfoils altering the aerodynamic characteristics for enhanced performance within different flight regimes [1]. Many researchers have also investigated position

J. G. DeHaven · H. S. Tzou (✉)
Department of Mechanical Engineering, Structronics and Design Lab, University of Kentucky, Lexington, KY 40506-0503, USA
e-mail: hstzou@engr.uky.edu

and tracking control with shape-memory wires and springs [2,3]. Besides, SMAs have been embedded within a number of composite materials for reducing hoop stress within high-pressure vessels, active vibration and structural acoustic control through active strain energy tuning and/or active modal modification, shape control of composite beams, and control of wave propagation in rods [4–7]. The use of SMAs for controlling the clearance between the shroud and blade tip within the high-pressure turbine of a turbine engine has also been studied [8,9] recently.

There are several classifications associated with the shape-memory effect. The three most common effects are (1) *the one-way effect*, (2) *the two-way effect*, and (3) *the pseudoelastic effect*. SMAs are known for their phase transformations from austenite to martensite and vice versa [10]. The objective of this study is to evaluate the feasibility of using SMAs for controlling the static deflection and vibration of cylindrical shells applied to turbine-engine control. Shape-memory alloys were chosen because of their ability to generate large forces as previously mentioned. This ability is very desirable for cases where the shell is relatively stiff and quasi-static deflection may be more important than the vibration control [8,9]. Note that, while the current SMAs are not as practical for vibration control because of their inability to cycle at high frequencies, this hurdle may change depending on the type of heating and cooling employed and the use of other metal compositions resulting in different SMAs with different abilities. A mathematical model of cylindrical shells coupled with SMA ring actuators at critical locations is formulated. Closed-form solution of the mnth modal response with arbitrary SMA control forces is derived in the modal domain, followed by control of input temperature profiles using the shaping and phase-shift techniques. Numerical solutions to evaluate shell response controlled by regulated SMA inputs are then provided and their control effectiveness evaluated.

2 Mathematical model of SMA coupled cylindrical shell panels

Figure 1 illustrates a cylindrical shell panel and two SMA actuator segments fitted to the shell panel. These ring segments are made of SMA wires or ribbons running across the cylindrical shell panel circumferentially and their number and placement along the length is determined by the shell modes to be controlled. These SMAs are strategically placed in the high-strain regions observed from distributed neural signals [11].

In order to determine control effects of cylindrical shell panels with shape-memory ring segments, SMA actuation forces integrated with dynamic equations of a cylindrical shell panel must be evaluated first. (Detailed SMA actuation mechanism will be discussed next.) Open-loop dynamic equations of cylindrical shells can be written as [12], [13, pp. 338–344]

$$\frac{\partial N_{xx}^{m}}{\partial x} + \frac{1}{R}\frac{\partial N_{\psi x}^{m}}{\partial \psi} + q_x - \rho h \ddot{u}_x = 0, \tag{1}$$

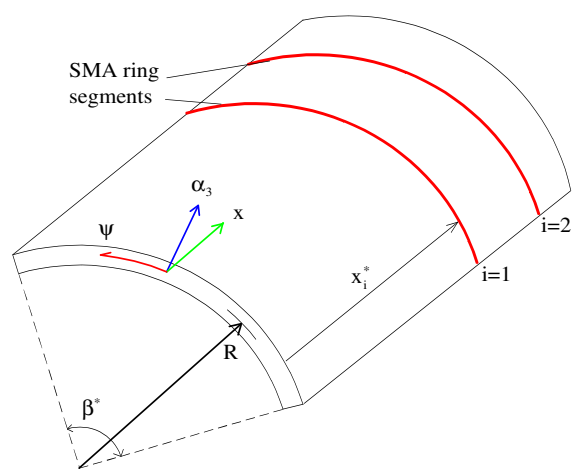

Fig. 1 A cylindrical shell panel with SMA ring Actuators

$$\frac{\partial N^m_{x\psi}}{\partial x} + \frac{1}{R}\frac{\partial N_{\psi\psi}}{\partial \psi} + \frac{1}{R}\frac{\partial M^m_{x\psi}}{\partial x} + \frac{1}{R^2}\frac{\partial M_{\psi\psi}}{\partial \psi} + q_\psi - \rho h \ddot{u}_\psi = 0, \tag{2}$$

$$\frac{\partial^2 M^m_{xx}}{\partial x^2} + \frac{2}{R}\frac{\partial^2 M^m_{x\psi}}{\partial x \partial \psi} + \frac{1}{R^2}\frac{\partial^2 M_{\psi\psi}}{\partial \psi^2} - \frac{N_{\psi\psi}}{R} + q_3 - \rho h \ddot{u}_3 = 0, \tag{3}$$

where N_{ij} and M_{ij} are the membrane force per unit length, and the bending moment per unit length, respectively; R is the shell radius; q_i is the external input in the i^{th} direction; ρ is the mass density; h is the shell thickness; and $\ddot{u}_x$ is the acceleration. Those terms with the superscript m are the mechanical forces and moments, while those without superscripts $N_{\psi\psi}$ and $M_{\psi\psi}$ contain both mechanical loads, superscript m, and loads from the actuating force, superscript a, resulting from the SMA ring actuators. Circumferential membrane force and moment $N_{\psi\psi}$ and $M_{\psi\psi}$ are respectively defined as

$$N_{\psi\psi} = N^m_{\psi\psi} - N^a_{\psi\psi} \quad and \quad M_{\psi\psi} = M^m_{\psi\psi} - M^a_{\psi\psi}. \tag{4, 5}$$

The SMA ring segments are stretched in the martensite phase to a certain percent strain below the martensite yield strain and they are attached to the shell panel. When these SMA ribbons, wires or ring segments are heated above the austenite start and finish temperatures, phase transformation to austenite will occur. The SMA tends to recover its strain even though no apparent detwinning (occurs when strain is generated beyond the martensite yield limit) of the martensite variants have occurred. The SMA wire will try to constrict, assuming the shell is sufficiently rigid, and it will not be able to recover much of this strain, thus causing the forces and bending moments in the circumferential direction represented by $N^a_{\psi\psi}$ and $M^a_{\psi\psi}$.

Since deflections normal to the shell are much more significant (i.e., $u_3 >> u_{\mathrm{x}}$ and u_ψ) and important to the clearance control, only the transverse equation, Eq. 3, is considered in future analysis. Assuming no other external influences ($\mathrm{q}_3 = 0$) and substituting Eqs. 4 and 5 in Eq. 3 yields

$$\frac{\partial^2 M^m_{xx}}{\partial x^2} + \frac{2}{R}\frac{\partial^2 M^m_{x\psi}}{\partial x \partial \psi} + \frac{1}{R^2}\frac{\partial^2 \left(M^m_{\psi\psi} - M^a_{\psi\psi}\right)}{\partial \psi^2} - \frac{\left(N^m_{\psi\psi} - N^a_{\psi\psi}\right)}{R} - \rho h \ddot{u}_3 = 0. \tag{6}$$

Equation (6) can be rearranged and leaves the terms in brackets to be labeled as Q_3 (i.e., induced control actions) which will be used later in the next section for the forced harmonic analysis, i.e.,

$$\frac{\partial^2 M^m_{xx}}{\partial x^2} + \frac{2}{R}\frac{\partial^2 M^m_{x\psi}}{\partial x \partial \psi} + \frac{1}{R^2}\frac{\partial^2 M^m_{\psi\psi}}{\partial \psi^2} - \frac{N^m_{\psi\psi}}{R} + \left[\frac{N^a_{\psi\psi}}{R} - \frac{1}{R^2}\frac{\partial M^a_{\psi\psi}}{\partial \psi^2}\right] - \rho h \ddot{u}_3 = 0. \tag{7a}$$

And set

$$Q_3 = \frac{N^a_{\psi\psi}}{R} - \frac{1}{R^2}\frac{\partial M^a_{\psi\psi}}{\partial \psi^2}. \tag{7b}$$

Again, this Q_3 is associated with the SMA-induced control actions to be used in modal force and modal control equation later. SMA induced control force and moment $N^a_{\psi\psi}$ and $M^a_{\psi\psi}$ are defined next.

3 SMA induced forces and moments

As discussed previously, SMA rings or ribbons are used in the shell control. Based on the one-dimensional (1D) *two way* shape-memory effect, the constitutive equation can be written in terms of stress T, strain S, elastic modulus Y, and martensite volume fraction ξ [2]:

$$T = \begin{cases} [Y_A - (Y_A - Y_M)\ \xi]\ S & 0 \leqslant S < S_M^y; \\ [Y_A - (Y_A - Y_t)\ \xi]\ S + \xi\ (Y_t - Y_M)\ S_M^y & S_M^y \leqslant S < S_M^d; \\ [Y_A - (Y_A - Y_d)\ \xi]\ S + \xi\ (Y_t - Y_M)\ S_M^y + (Y_d - Y_t)\ S_M^d & S_M^d < S. \end{cases} \tag{8}$$

where subscripts M, A, t, and d stand for martensite, austenite, twinned and detwinned martensite states, respectively. The strains at specific points on the stress–strain curve S_M^y and S_M^d denote the yield strain of twinned martensite and the minimum strain of detwinned martensite, respectively. The martensite volume fraction describes the amount of martensite present within the shape-memory material at a given moment; it is defined as a number between 0 and 1, 1 being 100% martensite and 0 being 0% martensite or 100% austenite. The transformation kinetics governing the evolution of the martensite volume fraction ξ are given by Dutta et al. [14] and defines the martensite volume fraction only as a function of temperature θ:

$$\frac{\mathrm{d}\xi}{\mathrm{d}\theta} = \begin{cases} \dfrac{1 - \xi - h_-(\theta)}{h_-(\theta) - h_+(\theta)} g_+(\theta) & \dot{\theta} \geq 0; \\ \dfrac{h_+(\theta) + \xi - 1}{h_-(\theta) - h_+(\theta)} g_-(\theta) & \dot{\theta} < 0. \end{cases} \tag{9a}$$

The initial condition for the differential equation is $\xi(0) = 1$. The functions g and h are given by Gaussian probability distribution functions and error functions erf$(\cdot)$.

$$g_{+/-}(\theta) = \frac{1}{v_{+/-}\sqrt{2\pi}} \exp\left(-\frac{\left(\theta - m_{+/-}\right)^2}{2v_{+/-}^2} \right); \tag{9b}$$

$$h_{+/-}(\theta) = \frac{1}{2}\left[1 + \mathrm{erf}\left(\frac{\theta - m_{+/-}}{v_{+/-}\sqrt{2}} \right) \right]. \tag{9c}$$

These functions are characterized by the mean $m_{+/-}$ and the standard deviation $v_{+/-}$, where the values for these are based on transformation temperatures of the SMAs and the +/− subscripts stand for increasing and decreasing curves respectively. $N_{\psi\psi}^a$ and $M_{\psi\psi}^a$ can now be defined in terms of the SMA force per unit length, and bending moment per unit length, respectively. Using the constitutive relation, Eq. 8, and transformation kinetics for the martensite volume fraction ξ, Eq. 9, yields the control force and moment.

$$N_{\psi\psi}^a = Y_s S W \quad \text{and} \quad M_{\psi\psi}^a = r_\psi^a Y_s S W, \tag{10, 11}$$

where S is the 1D strain in the martensite phase for the SMA ring segment; W is the width of the SMA ring or ribbon segment; r_ψ^a is the bending moment arm in the ψ-direction (distances measured from the neutral surface of the shell to the mid-surface of the actuator); and Y_s is the elastic modulus for the SMA defined as

$$Y_s = [Y_A - (Y_A - Y_M)\xi]. \tag{12}$$

A constant strain value S will be used as an approximation because it is really dependent on the shell behavior. If the shell is very flexible, like being made of thin rubber, very little force will be applied by the SMA during its transformation from martensite to austenite and the SMA will likely recover all of its strain thus $S = 0$. Or if the shell is very stiff, such as relatively thick steel, a very large force will be applied by the SMA to the shell during the transformation from martensite to austenite because the SMA is being restrained from recovering the strain. It is assumed that the strain S is constant for a specific shell structure. Formulation of open-loop forced response equations to evaluate how the SMA ring segments controlling unwanted external excitations is derived next.

4 Open-loop dynamic equation with SMA control forces

The modal-expansion method is a means for evaluating the dynamic response of shell deflections from the equations of motion via an infinite series of all participating modes. The amount of participation of each mode is determined

by a corresponding modal participation factor η_{mn}. Thus, the complete shell response can be represented by [15, p. 200]

$$u_i(\alpha_1, \alpha_2, t) = \sum_{m=1}^{\infty} \sum_{n=1}^{\infty} \eta_{mn}(t) U_{imn}(\alpha_1, \alpha_2). \tag{13}$$

Here u_i are the total response functions for the shell deflections in the i-directions. The subscript $i = 1, 2, 3$ refers to the in-plane and transverse directions, or $i = x, \psi, 3$ for the cylindrical shell panel in this analysis. The m and n subscripts refer to the mth and nth wave numbers related to the longitudinal and circumferential directions respectively and U_{imn} are the mode shape functions in the ith directions for the (m, n)th mode. The modal participation factors are determined from the modal dynamic equation

$$\ddot{\eta}_{mn} + \frac{\lambda}{\rho h}\dot{\eta}_{mn} + \omega_{mn}^2 \eta_{mn} = F_{mn}, \tag{14a}$$

and

$$F_{mn} = F_{mn}^m + F_{mn}^a, \tag{14b}$$

where λ is the shell's damping ratio, ω_{mn} is the natural frequency for the (m, n)th mode, F_{mn}^a is the SMA control force from the SMA ring segments, and F_{mn}^m is defined by the external loadings q_i. The general form for F_{mn} with the loading only normal to the shell (i.e., $q_i = q_3$) is defined as

$$F_{mn} = \frac{1}{\rho h N_{mn}} \int_{\alpha_1} \int_{\alpha_2} (q_3 + q_3^a) U_3 A_1 A_2 \mathrm{d}\alpha_2 \mathrm{d}\alpha_1, \tag{15}$$

where A_1 and A_2 are the Lamé parameters where $A_1 = A_x = 1$ and $A_2 = A_\psi = R$ for cylindrical shells. In this analysis, the limits of integration are from 0 to L in the x-direction (α_1) and 0 to β^* in the ψ direction (α_2) for a cylindrical-shell panel. The transverse-mode shape function U_3 of a simply supported cylindrical shell panel is

$$U_3 = C \sin\left(\frac{m\pi x}{L}\right) \sin\left(\frac{n\pi \psi}{\beta^*}\right). \tag{16}$$

And, thus,

$$N_{mn} = \int_{\alpha_1} \int_{\alpha_2} U_3^2 A_1 A_2 \mathrm{d}\alpha_2 \mathrm{d}\alpha_1 = \frac{RL\beta^*}{4}. \tag{17}$$

Note that q_3^a represents a summation of control forces derived from multiple SMA ring segments placed at critical locations depending on the mode (m, n). The SMA actuation is modeled as line loadings along the circumference of the cylindrical shell panel. Recall that $Q_3 = \frac{N_{\psi\psi}^a}{R} - \frac{1}{R^2}\frac{\partial M_{\psi\psi}^a}{\partial \psi^2}$ represents the control force/moment in the shell's transverse dynamic equation. However, the modal control force q_3^a is for a specific mode, which is considered negative because the SMA ring segments constrict the forces in the downward (or negative) transverse (3) direction. Thus, the total actuation of N SMA ring segments becomes

$$q_3^a = -\sum_{i=1}^{N} \frac{Q_3}{A_x} \delta\left(x - x_i^*\right), \tag{18}$$

where x_i^* represent these SMA critical locations depending on the mode be controlled and N is the total number of SMA rings. Substituting (16–18) in (15) gives the total control action induced by N SMA ring actuators for the (m, n)th mode.

$$F_{mn}^a = -\frac{4}{\rho h RL\beta^*} \int_0^L \int_0^{\beta^*} \left[\sum_{i=1}^{N} \delta\left(x - x_i^*\right) \left[\frac{N_{\psi\psi}^a}{R} - \frac{1}{R^2}\frac{\partial^2 M_{\psi\psi}^a}{\partial \psi^2}\right] \cdot \sin\left(\frac{m\pi x}{L}\right) \sin\left(\frac{n\pi \psi}{\beta^*}\right) R\right] \mathrm{d}\psi \mathrm{d}x. \tag{19}$$

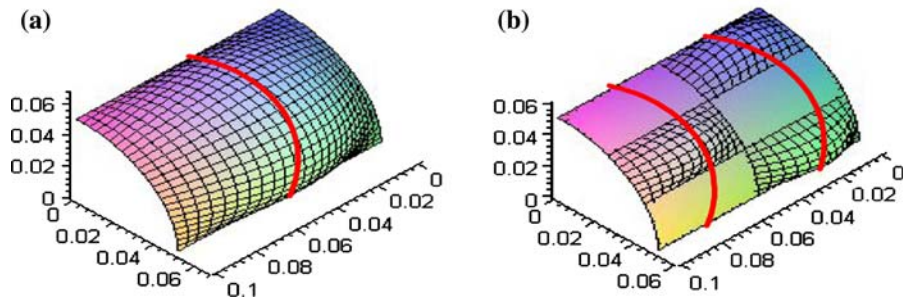

Fig. 2 Placements of SMA ring actuators for (**a**) (1,1) mode and (**b**) (2,3) mode of a 90° cylindrical shell panel) (Red line denotes the SMA ring actuator)

Since $M^a_{\psi\psi}$ is not a function of ψ, the second partial of $M^a_{\psi\psi}$ with respect to ψ becomes zero. This reduces the total control action, Eq. 19, to the following

$$F^a_{mn} = -\frac{4}{\rho h R L \beta^*} \int_0^L \int_0^{\beta^*} \left[\sum_{i=1}^{N} \delta\left(x - x_i^*\right) N^a_{\psi\psi} \cdot \sin\left(\frac{m\pi x}{L}\right) \sin\left(\frac{n\pi\psi}{\beta^*}\right) \right] \mathrm{d}\psi \mathrm{d}x. \tag{20}$$

Integration along the shell length in the x-direction from 0 to L and over the shell circumference from 0 to β^* yields

$$F^a_{mn} = \frac{4N^a_{\psi\psi}}{\rho h R L n\pi} \sum_{i=1}^{N} \sin\left(\frac{m\pi x_i^*}{L}\right) \left[\cos n\pi - 1\right], \tag{21}$$

where the last term in the brackets:

$$\left[\cos\left(\mathrm{n}\pi\right) - 1\right] = \begin{cases} -2 & n = 1,\ 3,\ 5, \ldots \\ 0 & n = 0,\ 2,\ 4, \ldots \end{cases} \tag{22}$$

indicates that the control action is only effective to the odd circumferential modes of the shell system, while the control action to all even modes is ineffective. Thus, rewriting the control force becomes

$$F^a_{mn} = -\frac{8N^a_{\psi\psi}}{\rho h R L n\pi} \sum_{i=1}^{N} \sin\left(\frac{m\pi x_i^*}{L}\right) \quad n = 1,\ 3,\ 5, \ldots \tag{23}$$

Now the SMA-induced control action F^a_{mn} for the (m, n)th shell mode is defined. The open-loop modal dynamic equation, Eq. (14), can be solved for the modal participation factor to evaluate the effect of the SMA control forces on the total shell dynamics, with or without external excitation F^m_{mn} derived from the transverse loading q_3. Figure 2 illustrates two odd-mode actuator configurations based on the modal-strain behavior [11]. For example, in order to control the (1,1) mode, one SMA segment is needed and it should be placed at the half-way point along the length (x-direction) of the shell, Fig. 2a; or, in order to control the (2,3) mode, two SMA segments are needed and should be placed at the one-fourth and three-fourths positions along the length of the shell, Fig. 2b.

In this study, the SMA-induced control force is used to counteract a sinusoidal periodic input. However, since the SMA behavior is highly nonlinear, regulation of temperature profile and phase is carried out to evaluate the control effectiveness presented later. Also, since a closed-form solution could not be obtained because of the complexity and nonlinearity of the martensite volume fraction, Heun's method, which is equivalent to a second-order accurate Runge–Kutta scheme, is used in a FORTRAN program to solve the system differential equations for the martensite volume fraction and the modal participation factor. These results are presented in the next section.

5 Controlled response of cylindrical shell panels

A cylindrical shell panel fitted with SMA ring actuators was illustrated in Fig. 1. Control effectiveness of a 90° cylindrical shell with temperature regulated SMA actuation is evaluated based on the SMA coupled closed-loop modal

Table 1 Defining shell-material properties and geometry

Cylindrical shell panel	Steel material properties and shell geometry
Elastic modulus, Y	30.0×10^6 psi
Mass density, ρ	7.35×10^{-4} s^2 lb/in
Damping ratio, ζ	0.02
Poisson's ratio, μ	0.3
Curvature angle, β^*	90°
Radius, R	1.9685 in
Length, L	3.937 in
Shell thickness, h	0.03937 in

Table 2 Defining actuator material properties and geometry [14]

Shape-memory ring segments	Material properties and ring geometry
Austenite modulus, Y_A	5209580 psi
Martensite modulus, Y_M	2970521 psi
Mean +, m_+	78.9°C
Mean −, m_-	34°C
Standard deviation +, v_+	11.2°C
Standard deviation −, v_-	5.8°C
Initial strain, S_o	0.001
Actuator width, w	0.125 in

equation and solution procedures derived previously. It is assumed that a sinusoidal pressure variation is imposed to the cylindrical shell and SMA actuators are used to cancel or minimize the shell-oscillation. Shell-material properties and geometric dimensions are listed in Table 1; material properties and geometry of the shape-memory ring segments are listed in Table 2. Before continuing, it should be noted that the present shape-memory alloys are not suitable for high-frequency applications. Although results presented here are performed using data from nickel–titanium (NiTi) SMAs, this study is eventually a "proof of concept or methodology" investigation designed for future shape-memory materials suited to faster phase transformations and less hysteresis in regard to the martensite volume fraction (i.e., martensite and austenite finish temperatures much closer together). The method of heating/cooling setup to this cylindrical shell panel and shape-memory ring segment setup is also equally important in order to be applied to high-frequency applications. In this study, the excitation frequency is set at 79.58 Hz that is "somehow" achievable for current NiTi actuators, if an effective heating/cooling technique is implemented.

As discussed previously, when using the modal-expansion method to represent the complete open-loop response for shell deflections, the goal is to minimize or cancel the modal oscillation for each mode (m, n) via SMA actuation forces to counter the unwanted external excitations—a sinusoidal input in this case. However, a sinusoidal temperature input to the SMA does not result in a sinusoidal force response due to its complex phase transformation and accordingly the control action does not line up exactly out-of-phase to cancel the sinusoidal excitation, i.e., no exact cancellation with the unwanted sinusoidal external excitation. This requires an input-shaping technique and in some cases minor tuning with respect to the phase or frequency of input. Following analyses demonstrate various temperature input functions with appropriate phase shift applied to the SMA ring segments to achieve a certain level of cancellation with the sinusoidal external excitation. Aside from the sinusoidal temperature input originally planned to control the SMA ring segments, a saw-tooth wave is tried and several different waveforms created by using a Fourier analysis applied to multiple exponential functions are also in development, but not presented here.

Originally a sinusoidal function for the temperature input to the SMA had been chosen to control the SMA's actuation in response to an external sinusoidal excitation. The specifications for this function are based on assuming the SMA is initially in the martensite phase and will take advantage of the full range of the given SMA's material properties, i.e., the SMA will be heated and cooled just above and below the austenite and martensite finish

temperatures, respectively. For the material properties of the NiTi SMA used, this means that the SMA is to be heated and cooled between 15 and 115°C. With these specifications, the temperature input function is defined as

$$\theta\,(t) = 50\cos\,(\omega t + \pi) + 65, \tag{24}$$

where θ represents the temperature (units of Celsius are used throughout), t is the time, and ω, the driving frequency (rad/s), is chosen to match the frequency of the external excitation, but in some cases it is tuned or the phase shift is changed to make the SMA response more synchronous with the external excitation.

The sinusoidal external excitation used here is a uniform pressure loading, but other types of loadings could be used depending on the environmental conditions, such as concentrated point and line loadings. For the forced vibration analysis using the modal expansion method this external excitation can be represented as:

$$F_{mn} = \frac{4}{\rho h R L \beta^*} \int_{\alpha_1} \int_{\alpha_2} q_3 U_3 A_1 A_2 \mathrm{d}\alpha_2 \mathrm{d}\alpha_1, \tag{25}$$

where q_3 is an external mechanical loading—a uniform pressure here. Since the external pressure loading is sinusoidal it can be represented as:

$$q_3 = P_1 \cos\,(\omega t) + P_2, \tag{26}$$

where P_1 and P_2 are constant values to determine amplitude and position above or below the x-axis (time), respectively. After integration over the cylindrical shell surface and substitution, the external loading F^m_{mn} can be represented as:

$$F^m_{mn} = \frac{16}{\rho h m n \pi^2}[P_1 \cos\,(\omega t) + P_2] \quad \begin{matrix} m = 1,\ 3,\ 5, \ldots \\ n = 1,\ 3,\ 5, \ldots \end{matrix} \tag{27}$$

Note that this type of loading only excites the odd modes circumferentially and longitudinally, similar to the SMA actuation. This is good, since it was found that only the odd ones can be controlled for the circumferential shell modes in the current actuator configuration.

The fundamental natural frequency of the 90° elastic shell panel is $\omega_{1mn} = 35{,}330.19$ rad/s or $f_{1mn} = 5{,}622.98$ Hz. Figure 3a shows the applied uniform sinusoidal pressure loading at $\omega = 500$ rad/s or $f = 79.58$ Hz; Figure 3b shows the response of the (1,1) modal participation factor η to this loading from the initial zero state. Note that Figure 3b is used as the standard response compared with that of various SMA temperature input waveforms discussed later. As discussed previously, the current shape-memory alloys are not suitable for high-frequency applications. However, it should be "manageable" at 79.58 Hz, if effective heating/cooling setup is used.

External loading freq. ω (rad/s)	Shell 1st natural freq. ω_{1mn} (rad/s)	Shell 1st natural freq. f_{1mn} (Hz)
500	35,330.19	56,22.98

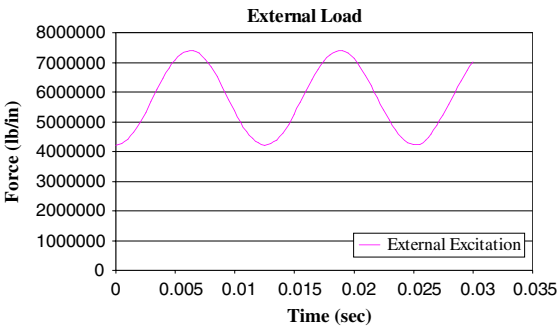

(a) Input data and uniform sinusoidal pressure loading.

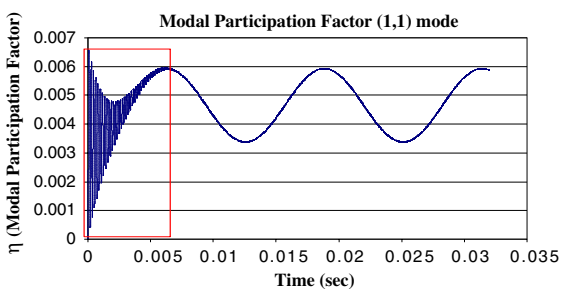

(b) Modal response to loading in **(a)**

Fig. 3 (**a**) Applied sinusoidal loading and (**b**) modal participation factor response of the (1,1) mode

The high-frequency oscillatory transient behavior observed at the beginning of Fig. 3b, enclosed by a red box,[1] is defined by the cylindrical shell panel's 1st natural frequency. Besides, it can be seen that the response of the modal participation factor resembles the applied loading at the steady state. Thus, to overcome the steady-state modal oscillation, the SMA actuator needs to deliver a "sinusoidal-like" actuation force to fully compensate the shell oscillation. However, due to the complexity and nonlinearity of SMA's phase transformation, this does not seem to be an easy task. Accordingly, input shaping and phase-shift techniques are applied to the temperature input of SMA actuators to minimize the shell oscillation. The following temperature input waveforms to be tested include regular sinusoids with and without phase shifts and a saw-tooth wave with phase shift. Reductions in modal amplitudes of cylindrical shell response subject to these controlled temperature profiles are compared.

5.1 Case 1: Sinusoidal temperature profile

A sinusoidal temperature profile (with and without phase shift) at the excitation frequency is first tested. The input frequency of the sinusoidal temperature profile is identical to the pressure frequency. If the actuator response were linear, this input could cancel out the pressure input and thus minimize the shell oscillation. However, since the SMA actuation depends on SMA's martensite/austenite fraction and its temperature-dependent stiffness, this exact cancellation is impossible, although the actuation force is significant. Figures 4 and 5 show results from a sinusoidal temperature waveform input to the SMA actuators, while a phase shift of $\pi/8$ is incorporated in Fig. 5. Note that the parts to each figure are: (a) a summary and the waveform of temperature input, (b) the martensite volume fraction response, (c) the applied loadings (including both sinusoidal external loading and SMA actuation force) to the shell, and (d) the response of the modal participation factor to both the uniform sinusoidal external excitation and the control force induced by the SMA actuator. This arrangement is used for all other regulated controlled responses presented later.

As Fig. 4 illustrates, a sinusoidal temperature profile does not generate a sinusoidal force profile and thus cancellation of sinusoidal pressure induced oscillation is not possible. With an external sinusoidal load advanced by a phase shift of $\pi/8$ as seen in Fig. 5, there is better cancellation of the modal participation factor, Fig. 5d. Again, there is a transient behavior at the beginning of the modal participation factor response in Fig. 5d, enclosed by a red box, but not in Fig. 4d. This appears to be caused by the phase shift applied to the external loading since there is no exact cancellation between the external loading and the SMA control force at the beginning, as seen in Fig. 5c, while there is exact cancellation at the beginning in Fig. 4c. Unfortunately only so much can be done with changing the phase shift to improve cancellation of the modal participation factor, which leads to the use of other temperature input functions to the SMA since a sinusoidal temperature input does not yield a sinusoidal SMA control force as seen in Fig. 4c and 5c.

Although inputting a sinusoidal temperature profile with proper phase shift tuning to the SMA provides better controlled response, but it still is not adequate enough to eliminate the modal response to an external sinusoidal uniform pressure loading. It also indicates that a temperature profile with a "sharper" slope increase could induce a "more sinusoidal" looking actuation. Thus, a saw-tooth waveform temperature input function is tested next.

5.2 Case 2: saw-tooth temperature profile

The saw-tooth waveform input for temperature profile is expressed as

$$\theta(t) = H_o - \sum_{\ell=1}^{\infty} \frac{8H}{\pi^2} \frac{1}{(2\ell-1)^2} \cos[(2\ell-1)\,\omega t], \tag{28}$$

where $H_o = 65$ is the average value of the waveform and $H = 50$ is the input amplitude. Figure 6a illustrates the saw-tooth temperature input waveform; Fig. 6b gives the martensite volume fraction response to this input; Fig. 6c

[1] Online version only.

SMA actuation freq. ω (rad/s)	External loading freq. ω (rad/s)	Shell 1st natural freq. ω_{1mn} (rad/s)	Shell 1st natural freq. f_{1mn} (Hz)
500	500	35330.2	5622.974

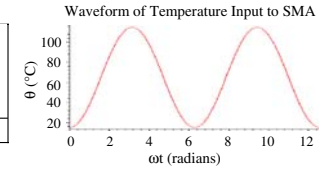

(a)

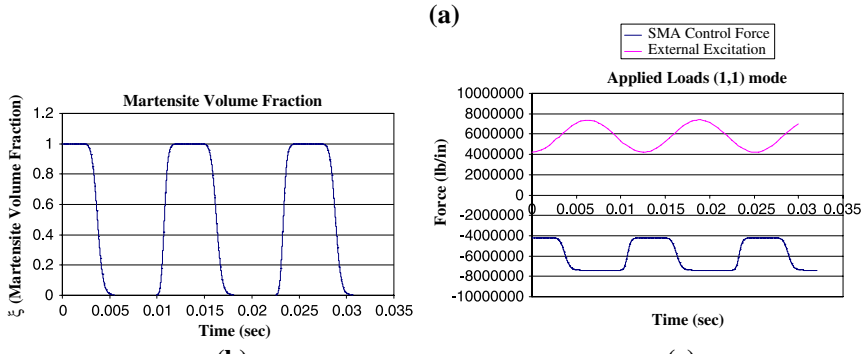

(b) **(c)**

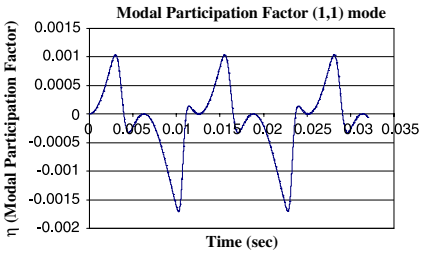

(d)

Fig. 4 Controlled response of shell's (1,1) mode (sinusoidal temperature input). (**a**) Input data and sinusoidal temperature profile to SMA. (**b**) Martensite volume fraction response to the temperature input. (**c**) Applied loadings (including both external sinusoidal loading and SMA control force) to cylindrical shell panel. (**d**) Modal response to applied loadings in (**c**)

shows the applied loads including the external sinusoidal pressure loading and the SMA control force; and Fig. 6d shows the response of the modal participation factor to the external sinusoidal uniform pressure loading and the control force induced by the SMA with the saw-tooth waveform and a phase advance of $\pi/6$ used as the temperature input to the SMA. The results are a little better than the sinusoid temperature inputs, but not significant enough to warrant desirable response. Again, the transient high frequency shell oscillation is observed in Fig. 6d, enclosed by the red box.[2] Variations on piecewise exponential functions transformed to Fourier series used as the temperature input profiles are under testing to further evaluate the SMA's control effectiveness.

To compare the control effectiveness of various temperature profiles, Table 3 summarizes the responses versus waveforms for various temperature inputs (with or without phase shift) to the SMA ring segments. Recall that all functions exploit full range of SMA martensite and austenite transformations (heating from 15 to 115°C and then back to 15°C for one complete cycle of the SMA), and the unwanted external excitation in every case is a sinusoidal uniform pressure loading applied to the cylindrical shell panel. The last column provides the reduction percentage of modal oscillation amplitude, which is reduced by the SMA regulated by various temperature profiles.

Analytical model based simulations in Figs. 4–6 and Table 3 suggest that the SMA ring segments are capable, to a certain extent, of controlling unwanted vibrations affecting cylindrical shell panels. For a sinusoidal pressure loading as the unwanted vibration, a sinusoidal temperature input with appropriate phase shift can be used as temperature input to the SMA for controlling the unwanted vibration, but the SMA actuators could be more effective

[2] Online version only.

SMA actuation freq. ω (rad/s)	External loading freq. ω (rad/s)	External loading phase shift (rad)	Shell 1st natural freq. f_{1mn} (Hz)
500	500	π/8	5622.974

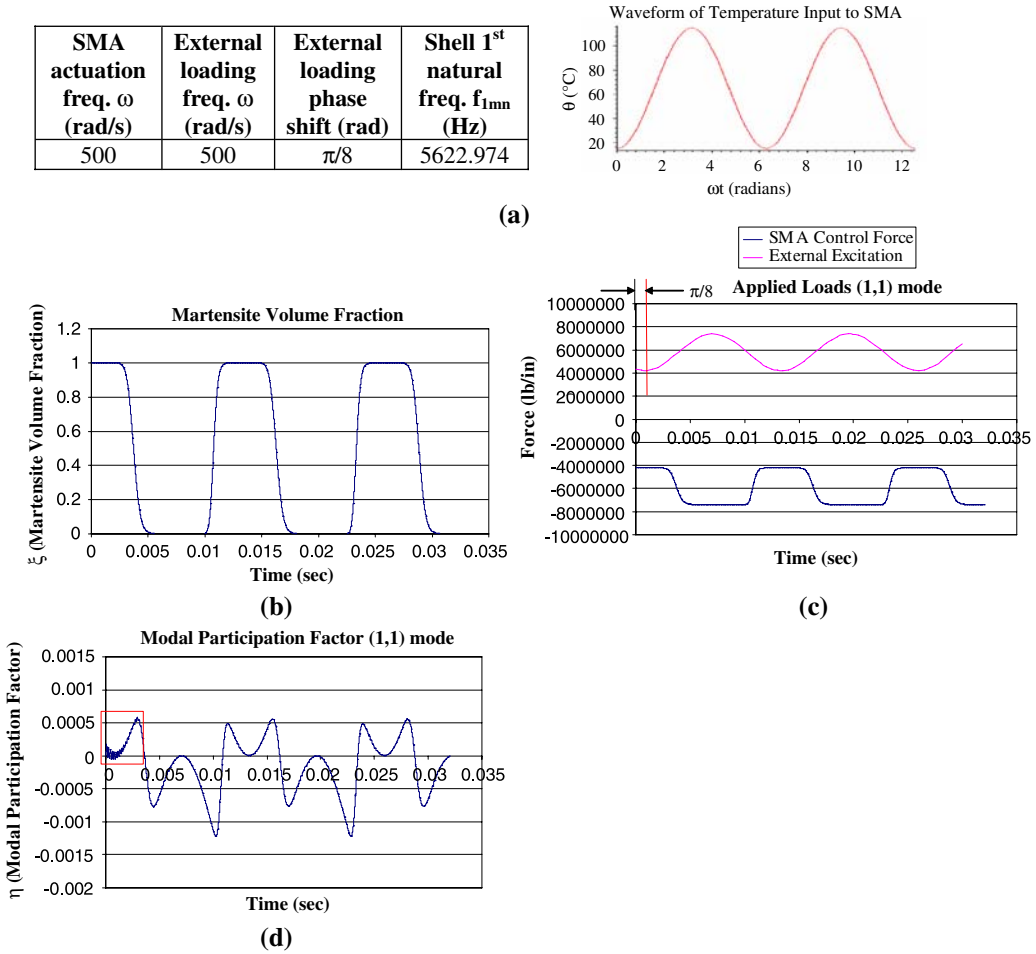

Fig. 5 Controlled response of shell's (1,1) mode (sinusoidal input with phase shift). (**a**) Input data and sinusoidal temperature profile, with phase shift, to SMA. (**b**) Martensite volume fraction response to the temperature input. (**c**) Applied loadings (including both external sinusoidal loading and SMA control force). (**d**) Modal response to applied loadings in (**c**)

with the appropriate temperature profile since the martensite response to a sinusoidal input is more like a square wave than a sine wave. Thus, a saw-tooth wave for temperature input, with a phase shift of $\pi/6$, improves the vibration cancellation, but not significantly greater than that induced by the sinusoidal temperature input, with a phase shift of $\pi/8$. Currently other temperature waveforms based on piecewise exponential functions and their martensite volume fraction responses to various temperature profiles are being tested and their results will be presented in the near future.

6 Conclusions

The purpose of this study has been to investigate the feasibility of manipulating temperature-input profiles, with or without phase shift, to SMA ring actuators and to evaluate the controlled responses of cylindrical shells subject to a sinusoidal excitation. Shape-memory alloys were chosen because of their ability to generate large forces due to SMA's phase transformation from martensite to austenite. The equations of motion and mode-shape functions for a simply supported cylindrical shell panel were given and SMA induced forces and moments were also integrated. With these expressions, and making the inclusion of multiple SMA rings segments with their placement determined

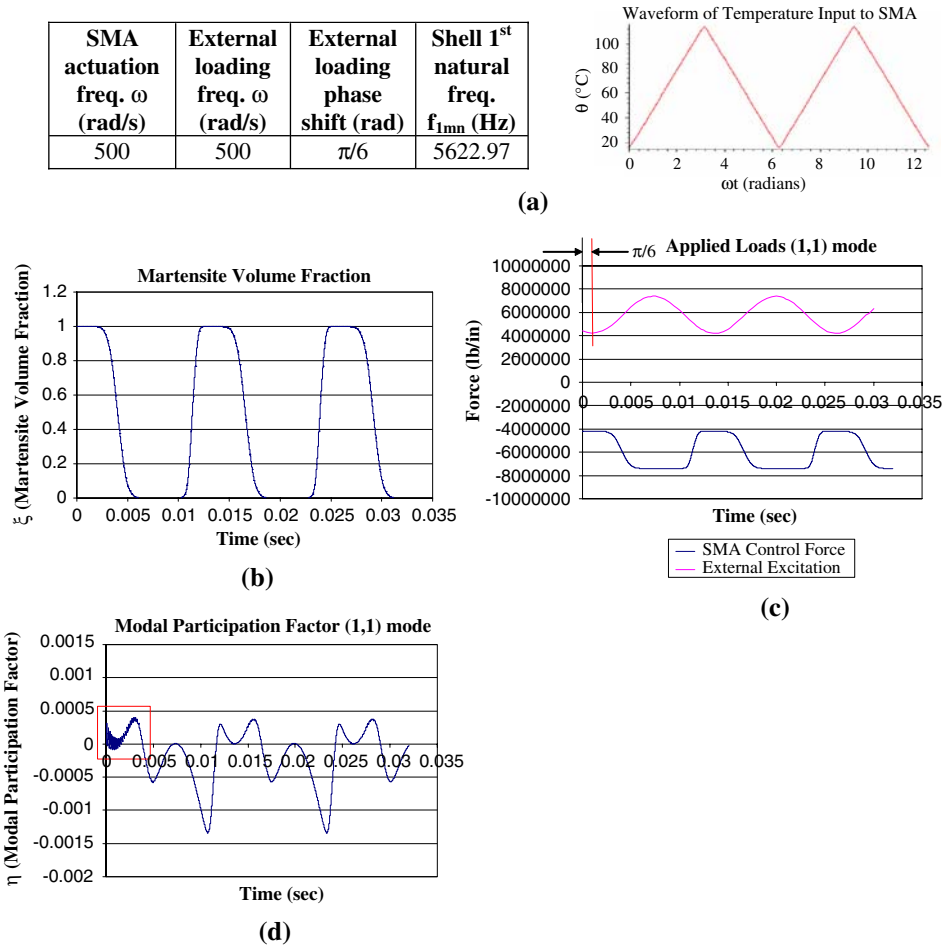

Fig. 6 Controlled response of shell's (1,1) mode (saw-tooth temperature profile with phase shift). (**a**) Input data and saw-tooth temperature waveform, with phase shift, to SMA; (**b**) Martensite Volume fraction response to the temperature input; (**c**) Applied loadings (including both external sinusoidal loading and SMA control force); (**d**) Modal response to applied loadings in (**c**)

Table 3 Controlled responses from various temperature input functions

Waveform	SMA actuation freq. ω (rad/s)	Shell 1st natural freq. ω_{1mn} (rad/s)	External loading phase shift (rad)	Reduction % of modal response
Sinusoidal	500	35330.19	0	−7.9
Sinusoidal	500	35330.19	$\pi/8$	30.2
Saw tooth	500	35330.19	$\pi/6$	32.9

by the mode number (m, n), the open-loop control forces of the SMA ring segments were determined using the modal-expansion method. Free and SMA-controlled responses were evaluated using the closed-form expressions of the modal equation incorporating mechanical and SMA induced excitations.

In order to test the ability of these SMA actuators to control unwanted external vibrations of cylindrical shells, a sinusoidal pressure loading has been used as the unwanted vibration and the force from the SMA actuators was applied with sinusoidal and saw-tooth temperature-input waveforms. With appropriate phase shift applied to these functions, the SMA actuators were capable of controlling the vibration, but not by a significant amount, due to complicated nonlinear SMA behavior. This is simply because the SMA force response to a sinusoidal temperature

input is not sinusoidal. Choosing other waveforms for temperature input profile to the SMA ring actuator, such as the saw-tooth waveform, gives more promising results, but still less satisfactory. Other temperature profiles, such as piecewise exponentials, are under consideration and testing.

Acknowledgements This research was supported, in part, by a grant from the NASA-Glenn Research Center, Program Managers: S.M. Arnold and H.-J. Lee. This support is gratefully acknowledged. Prof. Tzou would also like to express his appreciation to a Chair Professorship (NSC 95-2811-E-002-005) from the National Science Council, ROC (Taiwan) for his visit to Institute of Applied Mechanics (IAM) at the National Taiwan University (NTU) and supports from IAM and Prof. Peiling Liu (Director, IAM, NTU, 07/2003-06/2006).

References

1. Kudva JN, Appa K, Martin CA, Jardine AP, Sendeckyi G, Harris T, McGowan A, Lake R (1997) Design, fabrication, and testing of the DARPA/wright lab 'Smart Wing' wind Tunnel model. AIAA Paper 97–1198, April 1997
2. Madill DR, Wang D (1998) Modeling and L-2 stability of a shape memory alloy position control system. IEEE Trans Control Syst Technol 6(4):473–481
3. Ma N, Song G, Lee HJ (2003) Position control of SMA actuators with internal electrical resistance feedback. Smart Struct Mater 5049:46–54
4. Paine JSN, Rogers CA, Smith RA (1995) Adaptive composite materials with shape memory alloy actuators for cylinders and pressure vessels. J Intell Mater Syst Struct 6:210–219
5. Jia J, Rogers CA (1990) Formulation of a laminated shell theory incorporating embedded distributed actuators. Trans ASME 112:596–604
6. Baz A, Chen T, Ro J (2000) Shape control of NITINOL-reinforced composite beams. Compos Part B Eng 31:631–642
7. Chen T, Ruzzene M, Baz A (2000) Control of wave propagation in composite rods using shape memory inserts: theory & experiments. J Vib Control 6:1065–1081
8. Schetky M, Steinetz BM (1998) Shape memory alloy adaptive control of gas turbine engine compressor blade tip clearance. Smart Struct Mater 3326:346–354
9. Lattime SB, Steinetz BM (2002) Turbine engine clearance control systems: current practices and future directions. AIAA Paper 2002–3790, September 2002
10. Tzou HS, Lee H-J, Arnold SM (2004) Smart materials, precision sensors/actuators, smart structures and structronic systems. Mech Adv Mater Struct 11:367–393
11. DeHaven JG, Han Y, Tzou HS (2005) Transition of membrane/bending neural signals on transforming adaptive shells. J Vib Control 11(11):1397–1411
12. Tzou HS, Bao Y, Venkayya V (1996) Study of segmented transducers laminated on cylindrical shells, part 2: actuator patches. J Sound Vib 197(2):225–249 (SmaShlCd3x_ShlSMA2)
13. Tzou HS (1993) Piezoelectric shells-distributed sensing and control of continua, Chap. 9. Kluwer Academic Publishers, Boston/Dordrecht, pp 338–344
14. Dutta SM, Ghorbel FH, Dabney JB (2004) Dynamic modeling and control of hysteresis in a shape memory alloy actuator. Proceedings of IMECE04, 2004 ASME International Mechanical Engineering Congress and Exposition, Anaheim, California USA, November 13–20, 2004 (Paper No. IMECE2004–61849)
15. Soedel W (1981) Vibration of shells and plates. Marcel Dekker, Inc., New York and Basel, p. 200